Systematic effects important to separated-oscillatory-field measurements of the $n = 2$ Lamb shift in atomic hydrogen

A. Marsman, M. Horbatsch, Z. A. Corriveau, and E. A. Hessels*
Department of Physics and Astronomy, York University, Toronto, Ontario M3J 1P3, Canada

(Received 29 May 2018; revised manuscript received 5 July 2018; published 23 July 2018)

We evaluate a number of systematic effects that are important for an experimental microwave measurement of the $n = 2$ S-to-P intervals in atomic hydrogen. The analysis is important both for reevaluating the best existing measurement [S. R. Lundeen and F. M. Pipkin, Phys. Rev. Lett. **46**, 232 (1981)] of the $2S_{1/2}$-to-$2P_{1/2}$ Lamb shift and for a measurement that is ongoing in our laboratory. This work is part of a larger program to understand the several-standard-deviation discrepancies between various methods for determining the proton charge radius.

DOI: 10.1103/PhysRevA.98.012509

I. INTRODUCTION

The hydrogen Lamb-shift measurement has become important since it can determine, when compared to very precise theory [1], the charge radius of the proton. More precise determinations of this radius have now been performed using muonic hydrogen [2,3], but there is a large discrepancy between measurements made using ordinary hydrogen and muonic hydrogen. This discrepancy has become known as the proton size puzzle [4–6].

In this work, we evaluate possible systematic effects for a microwave separated-oscillatory-field (SOF) precision measurement of the atomic hydrogen $2S_{1/2}$-to-$2P_{1/2}$ Lamb shift. This interval was measured by Lundeen and Pipkin [7] in 1981 and is currently being remeasured by our group, with an aim to help resolve the proton size puzzle. We take advantage of the advances in computational power that have become available over the past decades to reevaluate the measurement of Lundeen and Pipkin and explore the implications for the proton size puzzle.

In particular, modern computers allow for a full modeling of the microwave fields based on the field-plate geometry. Additionally, modeling the time development of the density matrix from the time at which the atom is created to the time of detection is now possible. The density matrix calculations still require very intensive computations and we employ the SHARCNET computer cluster.

Of particular interest for this reevaluation is the possible effect of quantum mechanical interference. This effect requires a full density matrix modeling and would not have been included in the Schrödinger equation modeling of Refs. [7] and [8]. Such interference effects have been investigated by the present authors [9–15] and by others [16–26]. These investigations indicate that interference with a neighboring resonance, even if it is very distant, can lead to significant shifts for precision measurements.

Also, we reevaluate the ac Stark shifts and other possible systematic effects using our modeling of the microwave fields. Only small corrections are found relative to the analysis of Refs. [7] and [8].

Finally, we investigate the effect of a possible variation of microwave field strength as the microwave frequency is tuned across the resonance. We find that a correct and complete analysis gives a smaller correction than predicted by Refs. [7] and [8], and that this has a direct impact on the determination of the Lamb-shift interval.

II. MICROWAVE FIELD PROFILE

The microwave fields used for the separated-oscillatory-field measurement of Ref. [7] employed balanced transmission lines, as described further in Ref. [8]. In 1981, it was not computationally possible to simulate the full three-dimensional time-dependent fields, and therefore a simple two-dimensional dc model was used to estimate the fields. We have simulated the fields using the EMPIRE [27] software package. This field simulation gives the full three-dimensional field profile as well as its frequency dependence. Fortunately, the actual apparatus used to measure the Lamb shift has survived, as it was rescued from Harvard University by Lundeen in the early 1990's, and was passed on to our group several years ago when we began our Lamb-shift measurement. Thus, our field simulations are based on measurements of the actual plates that were used in the 1981 measurement.

That measurement used a total of eight configurations, for which the beam speed and separation between the two SOF fields (between the two sets of field plates) were varied. We have simulated fields for all eight configurations. A comparison of the fields used in the analysis by Refs. [7] and [8] and our simulations for configuration 1 is shown in Fig. 1. The profile shown is for 910 MHz, and one of the concerns we had was that this profile might vary with frequency. The simulations, however, show that the profile varies at only the 0.1% level over frequencies ranging between 780 and 1040 MHz. The actual frequency-dependent profiles are used for our density matrix

*hessels@yorku.ca

 ©2018 American Physical Society

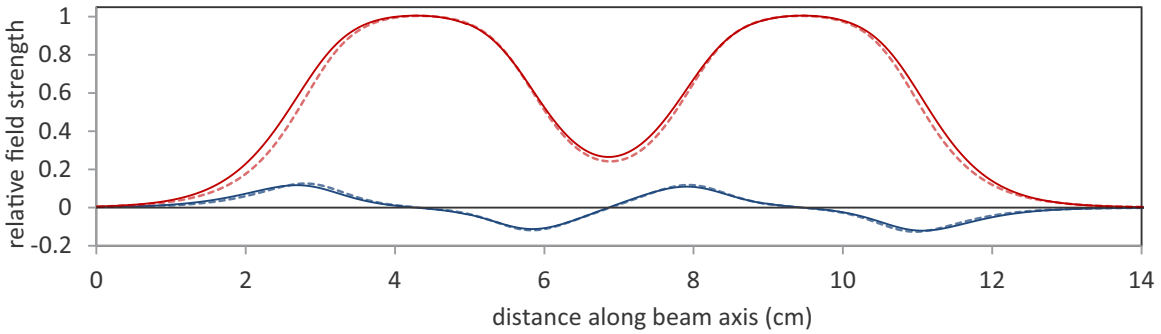

FIG. 1. The microwave field profile for configuration 1 of Ref. [8] (for the case where the two SOF fields are in phase). The dashed lines shows the field profile assumed in that work (which we have recalculated according to their prescription), and our simulated fields are shown by the solid lines. The field profiles shown are for a trajectory that is 2 mm above the beam axis. The larger graphed (in red) quantity is the vertical field component. The smaller quantity is the component of the field parallel to the atomic beam. The field profiles shown are for 910 MHz, but there is little variation in the profiles as a function of frequency.

computations, but the effect of the frequency dependence on the computed results is negligible.

III. DENSITY MATRIX CALCULATIONS

For this work, we perform density matrix calculations including all of the $n = 1$ and $n = 2$ states. These include the $1S_{1/2}(f = 0$ and $f = 1)$, $2S_{1/2}(f = 0, 1)$, $2P_{1/2}(f = 0, 1)$, and $2P_{3/2}(f = 1, 2)$ states, and all m_f sublevels, for a total of 20 states. Here, f is the quantum number associated with the total angular momentum for the hydrogen atom, and m_f is the projection of this angular momentum along the quantization axis. In a previous work, we extended the states to include higher n [15] and explored effects due to these higher-n states, but here we restrict ourselves to just the $n = 1$ and $n = 2$ states. In total, the density matrix ρ has 400 elements, with the 20 diagonal elements giving the populations and the 380 off-diagonal elements giving coherences. The coherences between the $n = 1$ and $n = 2$ populations can safely be ignored because the large energy difference between $n = 1$ and $n = 2$ leads to fast oscillations of these elements, and the oscillations cause a cancellation when averaged over physical processes that occur over time scales which include thousands or millions of these oscillations.

The density matrix equations follow the pattern given in Ref. [15], and include terms due to energy differences,

$$\dot{\rho}_{ba} = \frac{i(E_a - E_b)}{\hbar}\rho_{ba}, \tag{1}$$

terms due to the microwave electric field,

$$\dot{\rho}_{\rm aa} = i\frac{\langle a|e\vec{E}(t)\cdot\vec{r}\ |b\rangle^*}{\hbar}\rho_{\rm ab} - i\frac{\langle a|e\vec{E}(t)\cdot\vec{r}\ |b\rangle}{\hbar}\rho_{\rm ba}, \tag{2a}$$

$$\dot{\rho}_{\rm ba} = i\frac{\langle a|e\vec{E}(t)\cdot\vec{r}\ |b\rangle^*}{\hbar}(\rho_{\rm bb} - \rho_{\rm aa}), \tag{2b}$$

and terms for radiative decay of populations and coherences,

$$\dot{\rho}_{\rm aa} = \gamma_{\rm da}\rho_{\rm dd}, \tag{3a}$$

$$\dot{\rho}_{\rm dd} = -\gamma_{\rm da}\rho_{\rm dd}, \tag{3b}$$

$$\dot{\rho}_{\rm cd} = -\frac{\gamma_{\rm da} + \gamma_{\rm cb}}{2}\rho_{\rm cd}. \tag{3c}$$

For Eq. (3), it is assumed that states "a" and "b" are lower in energy than states "c" and "d" (to allow for radiative decay), and that γ_{ij} are the decay rates from state i to state j. All nonzero terms of the form of Eqs. (1)–(3) are included in the equations. Additional terms [28] are also included to account for quantum mechanical interference between radiative decays.

For the current work, we do not use the rotating-frame approximation, but simply integrate the time-dependent density matrix equations directly over the 400 ns time period that it takes the atoms to traverse the experimental apparatus (from the point where the atoms are created by charge exchange to the point of detection). The 400 ns includes a 35-ns-long preparation field at a frequency of 1110 MHz [which depletes the $2S_{1/2}(f = 1)$ population], the two 10-ns-long fields that form the SOF fields (see, e.g., Fig. 1), and a 10-ns-long field at 910 MHz which quenches the $2S_{1/2}(f = 0)$ population by driving it to the quickly decaying $2P_{1/2}$ state. These time intervals are reduced by a factor of $\sqrt{2}$ when the beam energy is increased from 50 to 100 keV. The amplitudes used for the three microwave field regions are 26, 11.4, and 11 V/cm, respectively. The radiative decay (Lyman-α fluorescence) is monitored during the quenching field, and this decay is the signal calculated by the density matrix equations. This signal is calculated for the case when the two SOF fields are in phase and when they are 180 degrees out of phase. The signals are also averaged over all phases for each quench region and over all phases for the average phase of the two SOF fields. The difference between the in-phase and 180-degree-out-of-phase signals produces the SOF interference signal that is used to measure the line center [see, e.g., the solid line in Fig. 2(b)]. The average of these two signals, which is referred to as $\overline{Q}$ [see, e.g., the solid line in Fig. 2(a)], is also calculated.

IV. QUANTUM MECHANICAL INTERFERENCE

The effect of quantum mechanical interference is included in the calculation by using the full density matrix equations, including all terms [28] that account for interference between radiative-decay paths. These additional terms have led to significant shifts in a number of investigations [9–26] of

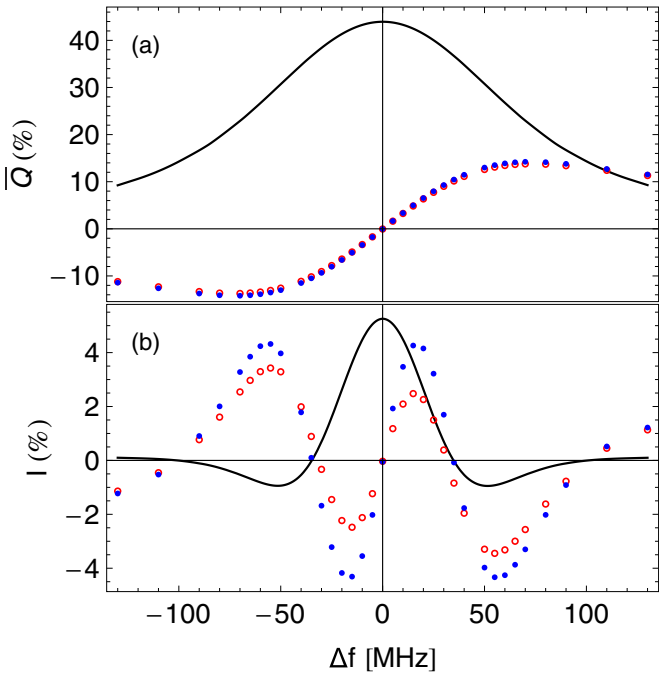

FIG. 2. Calculated line shapes for the case of configuration 1 with additional field-slope corrections. The line in (a) shows the quench signal $\overline{Q}$. The solid (blue) circles show the calculated correction (times 100) on the basis of Eq. (5), while the open (red) circles are the correction (times 100) from the explicit simulation using scaled fields. These are in close agreement and provide one line of evidence for a nonzero value of b. The line in (b) shows the calculated SOF signal which has a subnatural linewidth and is used for determining the line center. The solid (blue) circles show the calculated correction (times 1000) on the basis of Eq. (6), while the open (red) circles are the correction (times 1000) from the explicit simulation using scaled fields. The data are given vs frequency shift $\Delta f = \nu - \nu_0$, where ν_0 is the SOF line center obtained from the density matrix simulation. The frequency points are chosen to be those reported in Fig. 30 of Ref. [8].

quantum-interference effects on precision measurements. The effect of this quantum interference cannot be accounted for using an integration of the time-dependent Schrödinger equation, and therefore could not be investigated by the analysis of Refs. [7] and [8].

We have intentionally included the $2P_{3/2}$ states in our analysis, even though the $2S_{1/2}$-to-$2P_{3/2}$ transition is 9 GHz out of resonance with our microwave fields. An analysis [11] of a similar SOF measurement in the 2^3P states of helium showed that quantum mechanical shifts can be caused by even very far off-resonant transitions. Here, however, we see no quantum-interference shifts. That is, we observe identical line centers with or without the inclusion of the interference terms in the density matrix equations. We note that our earlier work [15] did show interference effects when higher-n states are included, but these shifts were due to processes that involved interferences between, for example, $2S$-to-$2P$ transitions and $3S$-to-$3P$ transitions, and resulted from the fact that these two $n = 3$ states can radiatively decay down to the two $n = 2$ states.

V. CALCULATED LINE-CENTER CORRECTIONS

We have used the density matrix equations, along with our simulated microwave fields, to calculate the line shapes for each of the eight configurations used in the Lundeen and Pipkin measurement. We have performed the simulation at the same set of frequencies as were used in the measurements and have determined the line center in the same manner as was used in the experiment. The SOF line centers are defined using the symmetric-points methods as given in Eq. (81) in Ref. [8].

The corrections to these SOF line centers that we observe in our simulations are separated into four categories. We first calculate the corrections that occur for atoms that are traveling along the central axis of the experiment, while also making the simplifying assumption that the $2S_{1/2}(f = 1)$ states have no initial population. The corrections are calculated for each of the eight configurations of the experiment and, in the final column of Table I, the weighted average of these values is given. The weighted average (for this and all other corrections) uses the weights originally employed by Lundeen and Pipkin [8], and these weights are listed explicitly in row 1 of the table. Our corrections in row 2 of Table I are compared to the similar corrections obtained in Ref. [8]. We find some small differences (of between 1 and 9 kHz) between our and their analysis for the eight configurations (as shown in row 4). However, the weighted averages differ by only 2.6 kHz, which is only marginally larger than the uncertainty that they assigned to this systematic effect.

The corrections for the fact that some atoms are displaced from the central axis of the beam line as they pass through the SOF fields have also been calculated using the full density matrix method. The off-axis trajectories could be important since, as shown in Fig. 1, they (unlike the on-axis trajectories) have components of the microwave electric field along the direction of the beam axis. As predicted in Ref. [8], the correction depends quadratically on how far the atoms are away from the central axis and, using their estimate that the rms distance is 1.265 mm, we obtain the corrections shown in row 5 of Table I. These agree within the stated uncertainties with the similar corrections in Ref. [8] and, as shown in row 6 of the table, the weighted average of the difference (row 7) between our corrections and theirs differs by only −1.4 kHz.

Similarly, the inclusion of initial populations in the $f = 1$ states leads to corrections (row 8) that are in reasonable agreement with Ref. [8]. The difference in the weighted average for this additional effect is completely negligible at only 0.2 kHz.

The final correction that we calculate is that due to a possible variation of microwave power as the microwave frequency is tuned across the resonance. The measured value for this field slope in Ref. [8] is −0.11(12)%/100 MHz. Our calculations for this effect are shown in row 11 of the table. Although our corrections agree to within the stated uncertainties for this effect calculated in Ref. [8] (shown in row 12), our corrections are systematically smaller by about a factor of three. The agreement between our corrections and theirs is due only to the large (more than 100%) uncertainty in their measured field slope.

TABLE I. A comparison of corrections predicted in this work to those found in Table 10 of Ref. [8] for the $2S_{1/2}(f = 0)$-to-$2P_{1/2}(f = 1)$ interval in atomic hydrogen. The corrections are in kHz, with uncertainties in the last digits in parentheses. Line-center corrections are calculated for all eight configurations used in Ref. [8], and weighted averages for the eight configurations are also calculated using the weights of Ref. [8] as listed in row 1.

Row	Systematic effect	Cfg. 1	Cfg. 2	Cfg. 3	Cfg. 4	Cfg. 5	Cfg. 6	Cfg. 7	Cfg. 8	Wt. avg.
1	Weight assigned by [8]	0.069	0.090	0.218	0.090	0.033	0.2955	0.182	0.0225	
2	$f = 0$ only; level power; on axis	–38.6	–27.0	–26.0	–22.0	–18.4	–25.1	–20.3	–18.1	–24.9
3	cf. Table 10 (row 2) [8]	–38(4)	–36(2)	–30(3)	–24(3)	–21(3)	–27(2)	–21(2)	–19(2)	–27.5(2.5)
4	Difference	–0.6	9.0	4.0	2.0	2.6	1.9	0.7	0.9	2.6
5	Additional off-axis correction	–6.2	–5.2	–5.2	–3.9	–3.6	–4.1	–3.7	–2.9	–4.4
6	cf. Table 10 (row 6) [8]	–6(4)	–3(2)	–3(2)	–3(2)	–3(2)	–3(2)	–2(1)	–2(1)	–3.0(1.9)
7	Difference	–0.2	–2.2	–2.2	–0.9	–0.6	–1.1	–1.7	–0.9	–1.4
8	Additional $f = 1$ correction	–0.1	0.0	0.0	0.0	0.0	–0.1	0.3	–0.1	0.0
9	cf. Table 10 (row 4) [8]	–4(1)	–2(1)	0(0)	0(0)	0(0)	1(0)	0(0)	0(0)	–0.2(0.2)
10	Difference	3.9	2.0	0.0	0.0	0.0	–1.1	0.3	–0.1	0.2
11	−0.11%/100 MHz field slope	2.3	0.8	0.3	0.2	0.1	0.2	0.0	0.2	0.4
12	cf. Table 10 (row 7) [8]	6(6)	4(2)	1(1)	1(1)	0(0)	–1(1)	0(0)	0(0)	0.8(1.2)
13	Difference	–3.7	–3.2	–0.7	–0.8	0.1	1.2	0.0	0.2	–0.4
14	Total corrections (this work)	–45.0	–32.2	–31.2	–25.9	–22.0	–29.2	–23.8	–21.0	–28.9
15	Total (rows 2, 6, 4, 7) [8]	–42(8)	–37(4)	–32(4)	–26(4)	–24(4)	–30(3)	–23(2)	–21(2)	–29.9(3.4)
16	Difference	–0.7	5.6	1.1	0.3	2.1	0.9	–0.7	0.2	0.9
17	Final centers with our corrections (minus 909 MHz)	926(10)	895(12)	911(8)	873(14)	875(23)	893(11)	887(14)	871(40)	
18	$b = 0.5(2)$%/100 MHz field slope	–10.4(4.2)	–3.5(1.4)	–1.2(0.5)	–1.0(0.4)	–0.6(0.2)	–0.8(0.3)	0.0(0.0)	–0.9(0.4)	–1.7(0.7)
19	cf. Table 10 (row 8) [8]	–25(10)	–18(7)	–9(3)	–6(2)	–2(1)	–5(2)	–2(1)	–2(1)	–7.8(3.0)
20	Difference	14.6	14.5	7.8	5.0	1.4	4.2	2.0	1.1	6.1
21	Final centers with our corrections including row 18 (minus 909 MHz)	916(11)	891(12)	910(8)	872(14)	874(23)	892(11)	887(14)	870(40)	
22	Our suggested corrected result									909.894(20) MHz

In row 14, we show the total of all four effects discussed. These are compared to the similar totals from Ref. [8] in row 15. The corrections agree to within the uncertainties given in the original work, and the weighted average of our total correction agrees with theirs to better than 1 kHz. The final line centers for each configuration (using our corrections) are shown in row 17 of the table. The results for the eight configurations are not in good agreement, with a standard deviation of 19 kHz, which is much larger than the uncertainties for most of the configurations. The reduced χ^2 for the eight configurations agreeing with their weighted average is 2.6, which is unacceptably large. One might be tempted to simply increase the uncertainty in the weighted average by the square root of this reduced χ^2 value; however, this procedure would simply mask the fact that the results in the eight configurations are not consistent and that an unknown systematic effect must be present and must be causing the inconsistency.

VI. ADDITIONAL FIELD SLOPE

Lundeen and Pipkin resolved the discrepancies between the centers for different configurations by noting that there were three lines of evidence that pointed to a larger than expected field slope, with an *additional* slope of $b = +0.5(2)$%/100 MHz (over and above the field slope directly measured and accounted for in row 7 of their Table 10 [8]). The increase in strength of the rf field as one scans in frequency across the line profile is described as

$$E_{\rm rf}(\nu) = E_0[1 + b\,(\nu - 910\,\text{MHz})]. \tag{4}$$

Based on the three lines of evidence, they add an *ad hoc* correction to their line centers based on b.

The first, and most statistically significant, evidence for the existence of an additional field slope b came from an analysis of the asymmetry (about the SOF line center) of the $\overline{Q}$ signal. Our analysis of their observed asymmetry agrees with their assessment of the implied b (as listed in column 2 in Table 14 of Ref. [8]). In particular, we verify their scaling of $\overline{Q}$ with field strength, which they used to determine b. The formula given for this scaling is

$$\overline{Q}(E_{\rm rf}, \nu) = \overline{Q}(E_0, \nu)\left(\frac{E_{\rm rf}(\nu)}{E_0}\right)^{2-\overline{Q}(E_0,\nu)}, \tag{5}$$

with $E_{\rm rf}(\nu)$ defined in Eq. (4). $\overline{Q}(E_0, \nu)$ is the quench signal observed with ν-independent electric-field strength E_0.

In Fig. 2(a), we show calculated line shapes and additional field-slope distortion for the case of configuration 1. It is obvious that Eq. (5) captures the quench signal correction appropriately since our direct simulation (open red points) agrees with the model (closed blue points).

The second line of evidence that they used to show that an additional field slope b was present is based on a postulated analogous equation to Eq. (5) for the scaling with field strength

of the SOF interference signal I, namely,

$$I(E_{\rm rf},\nu) = I(E_0,\nu)\left(\frac{E_{\rm rf}(\nu)}{E_0}\right)^{2-\overline{Q}(E_0,\nu)}. \quad (6)$$

In this case, our analysis shows that this scaling does not correctly predict the effect on the SOF signal due to a variation in rf field strength with frequency, and, therefore, does not properly describe the asymmetry caused by a field slope. Thus, the results in the third column of Table 14 of Ref. [8] give incorrect estimates of b.

The point is illustrated in Fig. 2(b), where the discrepancy between the actual simulation (red open circles) and the results based on Eq. (6) (blue closed points) is apparent. Note that despite the oscillatory character of the correction, there is a significant shift in the line center because the sign of the correction conspires with the sign of the slope of the SOF signal.

The third line of evidence that Lundeen and Pipkin used involves the SOF line centers themselves. They make the case that the inclusion of the larger field slope makes these line centers more consistent. We show the corrections that they applied in row 19 of Table I. However, because the scaling formula that they used, i.e., Eq. (6), does not agree with our analysis, we get a different (and about a factor of three smaller) effect due to a $b = 0.5\%/100$ MHz field slope, as shown in row 18 of the table. The weighted averages of the corrections differ by 6.1 kHz, as shown in row 20. More importantly, our corrections indicated in row 18 of the table do not serve to resolve the discrepancies between the line centers obtained for the eight configurations, as shown in row 21. The eight centers corrected for $b = 0.5\%/100$ MHz do not show acceptable agreement with each other, and the values in row 21 still have a standard deviation of 17 kHz.

VII. CORRECTED CENTER

Given our reanalysis of the systematic effects, we take the weighted average of the values in row 21 of Table I to be the best estimate of the center measured in that work. These values are plotted in Fig. 3(b), alongside the original values from Ref. [8]. The only significant disagreement that we find with the original analysis is the treatment of the field slope

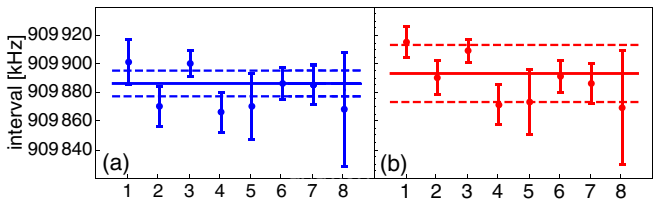

FIG. 3. Measured $2S_{1/2}(f=0)$-to-$2P_{1/2}(f=1)$ interval vs configuration number. (a) The published results of Ref. [8] along with their final quoted result (solid line) and assigned uncertainty range of ±9 kHz (dashed lines). (b) The results from the present analysis (row 21 in Table I), together with its weighted average and our final uncertainty of ±20 kHz. The present results (b) are primarily different from the original data [8] shown in (a) because the additional field-slope correction applied to the SOF line centers (row 8 in Table 10 of Ref. [8]) is replaced by fully modeled results (shown in line 18 of our Table I).

and, in particular, the *ad hoc* correction due to an additional field slope, given by Eq. (6). Our reanalysis of this effect leads to a correction of +6 kHz in the resonance center (row 20), which (along with another +1 kHz correction from all other effects, as shown in row 16) changes the measured value for the $2S_{1/2}(f=0)$-to-$2P_{1/2}(f=1)$ interval in atomic hydrogen from 909.887 to 909.894 MHz.

Four considerations need to be included in the assessment of the uncertainty in this measurement. The first consideration is the 9 kHz uncertainty from the original analysis of this measurement. The second consideration is the question as to whether any level of correction should have been made for the *ad hoc* additional slope b. Given that two of the lines of evidence indicated by Lundeen and Pipkin do not hold up in our reanalysis, it may not make sense to still make a correction. Since our analysis gives a correction of only 1.7 kHz for the additional field slope b, we assign an additional uncertainty of 1.7 kHz. The third consideration in the assignment of an uncertainty is the fact that with our reanalysis, the centers in the eight configurations no longer agree with each other. The standard deviation for the eight configurations is 17 kHz (or 19 kHz if we do not make an *ad hoc* correction for b). We assign an additional uncertainty equal to this standard deviation since it is not clear, without identifying a cause for the discrepancy, which of the configurations gives the correct center for the interval.

When added in quadrature, the uncertainty from these three sources gives 20 kHz and is dominated by the standard deviation of the eight configurations. A final consideration is found in our previous work [15], in which we showed that the effect of higher-n states could be of the order of 10 kHz. Since the 20 kHz uncertainty assigned here is larger than the this 10 kHz scale, and since, as discussed in Ref. [15], we cannot calculate the actual shift caused by higher-n states present in the beam, we do not assess any additional uncertainty due to the possible effect from these states.

The final estimate for our reevaluation of the measured value for the $2S_{1/2}(f=0)$-to-$2P_{1/2}(f=1)$ interval is therefore 909.894(20) MHz. This value agrees (to within its uncertainty) with the original value of Refs. [7] and [8]. This estimation can be related to the determination of the proton charge radius and to the Rydberg constant [21,29,30] when taking into account precise quantum-electrodynamics theoretical predictions for the Lamb shift. The proton charge radius based on the present reevaluation results in a value of $R_p = 0.90(6)$ fm. Therefore, the result is consistent with both the larger radius suggested by CODATA [29] and the smaller radius suggested by some recent measurements [2,3,21].

VIII. CONCLUSIONS

We have reanalyzed the $H(n=2)$ Lamb-shift measurement made in 1981 by Lundeen and Pipkin, taking advantage of computing improvements in the intervening decades. Using a more sophisticated analysis of both the fields and the atomic physics processes, we find that we largely agree with their original analysis. We find, however, one correction to their analysis. In all, we suggest that their result should be corrected by 7 kHz and their uncertainty be increased to 20 kHz. The increased uncertainty makes the measurement consistent with both the small and large values of the proton charge radius that have been the subject of the recent proton radius puzzle.

The analysis performed in this work will directly apply to a measurement of the same interval that is ongoing in our laboratory.

ACKNOWLEDGMENT

This work is supported by NSERC and a York Research Chair and used SHARCNET for computation.

[1] For an overview of measurements of the hydrogen Lamb shifts and theoretical predictions, see Refs. [30] and [29]. See also Refs. [21] and [31] for two more recent measurements in atomic hydrogen.
[2] R. Pohl, A. Antognini, F. Nez, F. D. Amaro, F. Biraben, J. M. Cardoso, D. S. Covita, A. Dax, S. Dhawan, L. M. Fernandes *et al.*, Nature (London) **466**, 213 (2010).
[3] A. Antognini, F. Nez, K. Schuhmann, F. D. Amaro, F. Biraben, J. M. Cardoso, D. S. Covita, A. Dax, S. Dhawan, M. Diepold *et al.*, Science **339**, 417 (2013).
[4] J. C. Bernauer and R. Pohl, Sci. Am. **310**, 32 (2014).
[5] R. Pohl, R. Gilman, G. A. Miller, and K. Pachucki, Annu. Rev. Nucl. Part. Sci. **63**, 175 (2013).
[6] C. E. Carlson, Prog. Part. Nucl. Phys. **82**, 59 (2015).
[7] S. R. Lundeen and F. M. Pipkin, Phys. Rev. Lett. **46**, 232 (1981).
[8] S. R. Lundeen and F. M. Pipkin, Metrologia **22**, 9 (1986).
[9] M. Horbatsch and E. A. Hessels, Phys. Rev. A **82**, 052519 (2010).
[10] M. Horbatsch and E. A. Hessels, Phys. Rev. A **84**, 032508 (2011).
[11] A. Marsman, M. Horbatsch, and E. A. Hessels, Phys. Rev. A **86**, 012510 (2012).
[12] A. Marsman, M. Horbatsch, and E. A. Hessels, Phys. Rev. A **86**, 040501 (2012).
[13] A. Marsman, E. A. Hessels, and M. Horbatsch, Phys. Rev. A **89**, 043403 (2014).
[14] A. Marsman, M. Horbatsch, and E. A. Hessels, Phys. Rev. A **91**, 062506 (2015).
[15] A. Marsman, M. Horbatsch, and E. A. Hessels, Phys. Rev. A **96**, 062111 (2017).
[16] C. J. Sansonetti, C. E. Simien, J. D. Gillaspy, J. N. Tan, S. M. Brewer, R. C. Brown, S. Wu, and J. V. Porto, Phys. Rev. Lett. **107**, 023001 (2011).
[17] R. C. Brown, S. J. Wu, J. V. Porto, C. J. Sansonetti, C. E. Simien, S. M. Brewer, J. N. Tan, and J. D. Gillaspy, Phys. Rev. A **87**, 032504 (2013).
[18] C. J. Sansonetti, C. E. Simien, J. D. Gillaspy, J. N. Tan, S. M. Brewer, R. C. Brown, S. Wu, and J. V. Porto, Phys. Rev. Lett. **109**, 259901(E) (2012).
[19] P. Amaro, B. Franke, J. J. Krauth, M. Diepold, F. Fratini, L. Safari, J. Machado, A. Antognini, F. Kottmann, P. Indelicato, R. Pohl, and J. P. Santos, Phys. Rev. A **92**, 022514 (2015).
[20] D. C. Yost, A. Matveev, E. Peters, A. Beyer, T. W. Hänsch, and T. Udem, Phys. Rev. A **90**, 012512 (2014).
[21] A. Beyer, L. Maisenbacher, A. Matveev, R. Pohl, K. Khabarova, A. Grinin, T. Lamour, D. C. Yost, T. W. Hänsch, N. Kolachevsky, and T. Udem, Science **358**, 79 (2017).
[22] P. Amaro, F. Fratini, L. Safari, A. Antognini, P. Indelicato, R. Pohl, and J. P. Santos, Phys. Rev. A **92**, 062506 (2015).
[23] A. A. Buchheit and G. Morigi, Phys. Rev. A **94**, 042111 (2016).
[24] H. Fleurbaey, F. Biraben, L. Julien, J.-P. Karr, and F. Nez, Phys. Rev. A **95**, 052503 (2017).
[25] G.-P. Feng, X. Zheng, Y. R. Sun, and S.-M. Hu, Phys. Rev. A **91**, 030502 (2015).
[26] G.-W. Truong, J. D. Anstie, E. F. May, T. M. Stace, and A. N. Luiten, Nat. Commun. **6**, 8345 (2015).
[27] Computer code EMPIRE, Version 4.20, IMST GmbH, http://www.empire.de/main/Empire/en/home.php (unpublished).
[28] D. A. Cardimona and C. R. Stroud, Phys. Rev. A **27**, 2456 (1983).
[29] P. J. Mohr, D. B. Newell, and B. N. Taylor, J. Phys. Chem. Ref. Data **45**, 043102 (2016).
[30] M. Horbatsch and E. A. Hessels, Phys. Rev. A **93**, 022513 (2016).
[31] H. Fleurbaey, S. Galtier, S. Thomas, M. Bonnaud, L. Julien, F. Biraben, F. Nez, M. Abgrall, and J. Guéna, Phys. Rev. Lett. **120**, 183001 (2018).